Available online at www.sciencedirect.com
SCIENCE DIRECT®
Planetary and Space Science 51 (2003) 785–795
Planetary and Space Science
www.elsevier.com/locate/pss

Production of gyrating ions from nonlinear wave–particle interaction upstream from the Earth's bow shock: A case study from Cluster-CIS

C. Mazelle[a,*], K. Meziane[b], D. LeQuéau[a], M. Wilber[c], J.P. Eastwood[d], H. Rème[a], J.A. Sauvaud[a], J.M. Bosqued[a], I. Dandouras[a], M. McCarthy[e], L.M. Kistler[f], B. Klecker[g], A. Korth[h], M.B. Bavassano-Cattaneo[i], G. Pallocchia[i], R. Lundin[j], A. Balogh[d]

[a] *CESR, CNRS/UPS, 9 Avenue du Colonel Roche, BP 4346, 31028 Toulouse Cedex 4, France*
[b] *Physics Department, University of New Brunswick, P.O. Box 4400, Fredericton, NB, Canada E3B 5A3*
[c] *Space Sciences Laboratory, University of California, Berkeley, CA 94720, USA*
[d] *Imperial College, London, UK*
[e] *Earth and Space Sciences, University of Washington, Seattle 98195, USA*
[f] *University of New Hampshire, Durham, USA*
[g] *MPI, Garching, Germany*
[h] *MPAe, Katlenburg-Lindau, Germany*
[i] *CNR-IFSI, Frascati, Italy*
[j] *IRF, Kiruna, Sweden*

Received 20 November 2002; received in revised form 22 May 2003; accepted 22 May 2003

Abstract

We present observations of $E < 40$ keV/e backstreaming ions measured by the Cluster Ion Spectrometry experiment at 1–2R_E upstream of the bow shock. The ions are simultaneously observed at all three spacecrafts for which CIS measurements are available. The proton distributions are analyzed using 4 s time resolution. They are observed in association with low-frequency quasi-monochromatic waves with substantial amplitudes ($\delta\mathbf{B}/B \sim 1$). When the waves are present the ion distributions appear as gyrophase-bunched gyrating distributions while field-aligned beams are also observed just adjacent to the interval of wave occurrence. The gyrating distributions are observed at distances larger than an ion Larmor radius and they have pitch-angles inconsistent with a specular reflection mechanism at the bow shock. The properties of the ULF waves reveal that they are in cyclotron resonance with the ion parallel beams that could drive a right-hand ion/ion instability responsible for the wave occurrence. Moreover, the observed pitch-angles for the gyrating ion distributions are consistent with the theoretical value expected if they are produced by a coherent nonlinear wave–particle interaction.

Keywords: Planetary magnetospheres; Upstream waves and particles; Wave-particle interaction

1. Introduction

Several types of ion populations have been observed upstream of the Earth's bow shock (Bonifazi and Moreno, 1981a; Gosling et al., 1978; Paschmann et al., 1981; Gurgiolo et al., 1981). These population have been extensively studied and hypotheses have been put forward to explain their origin (Paschmann et al., 1980; Bonifazi and Moreno, 1981b; Gurgiolo et al., 1983; Lee, 1982). Ions beams of several keV collimated along interplanetary field lines have been observed upstream from the quasi-perpendicular shock (Bonifazi and Moreno, 1981a). Downstream of the field-aligned beam region, distributions characterized by a gyromotion around the magnetic field, i.e., a nonvanishing perpendicular bulk velocity with respect to the background magnetic field, have been reported. These gyrating ion distributions are nongyrotropic or nearly gyrotropic. Numerous studies concerning gyrating ions have been reported in earlier investigations mainly from ISEE 1 and 2 (Gosling et al., 1982; Thomsen et al., 1985; Fuselier et al., 1986b,c), AMPTE (Fazakerley et al.,

* Corresponding author.
E-mail address: christian.mazelle@cesr.fr (C. Mazelle).

0032-0633/$ - see front matter © 2003 Elsevier Ltd. All rights reserved.
doi:10.1016/j.pss.2003.05.002

1995) and WIND (Meziane et al., 1997, 2001; Mazelle et al., 2000). Gyrating ions are often observed in association with ULF waves having substantial amplitude (Fuselier et al., 1986c). The waves are right-handed and propagate nearly along the ambient magnetic field (e.g., Thomsen et al., 1985). It is believed that the ULF waves are excited through a beam plasma instability resulting from the propagation of field-aligned ions which precede them closer to the foreshock boundary (Gary et al., 1981).

Two mechanisms are put forward to explain the origin of gyrating ions. In one mechanism, a portion of the incoming solar wind are reflected in a specularly manner at the shock (Gosling et al., 1982; Gurgiolo et al., 1983). Solar wind specular reflection should produce nongyrotropic ion distribution. When propagating upstream, the bunched ions undergo gyrophase mixing within a few Earth radii from their source on the shock leading to nearly gyrotropic distribution function (Gurgiolo et al., 1983). Gyrotropic distribution have not been observed in 3D measurement; however, 2D measurements suggest their presence within $\sim 4R_E$ from the shock (Fuselier et al., 1986c). This indicates also that shock-produced nongyrotropic distributions are rarely observed beyond $\sim 4R_E$. Very few cases of ion distributions consistent with the hypothesis of specular reflection have been reported in the literature. (Gosling et al., 1982) reported first evidence of a specular reflection of a portion of the solar wind using the ISEE-FPE experiment and where ISEE was just upstream of the shock. An other event consistent with the specular reflection observed at $\sim 4R_E$ and in association with ULF waves has been reported by Thomsen et al. (1985). Furthermore, theoretically, for a given uniform magnetic field, the specular reflection mechanism occurs with the same efficiency independently of the shock geometry. However, as shown by Gosling et al. (1982), only particles reflected for $\theta_{Bn} < 45°$ (quasi-parallel geometry) have guiding centers oriented upstream, θ_{Bn} being the angle between the magnetic field and the local shock normal. In addition, because of kinematical considerations, only specularly reflected ions occurring for $\theta_{Bn} < 39.9°$ do not reencounter the shock and therefore escape upstream Schwartz et al. (1983). In presence of large amplitude ULF MHD waves near the shock front, always observed in association with gyrating ions, the bow shock θ_{Bn} varies substantially; it results that the shock may switch back and forth from quasi-parallel to quasi-perpendicular geometry (Greenstadt and Mellott, 1985). As theoretically shown by Fuselier et al. (1986a), this effect, depending upon the waves characteristics, inhibits the escape of specularly reflected ions. When the wave amplitude is high ($|\delta\mathbf{B}|/B_0 \approx 1$), the effect is relatively strong.

In the second mechanism, the produced waves through a beam-plasma instability can in turn trap the ions and cause the phase bunching of the distribution in what is called a beam disruption mechanism (Hoshino and Terasawa, 1985). Fuselier et al. (1986b) made a quantitative analysis of particle and monochromatic waves from ISEE data which strongly suggested that there was wave–particle interaction. They obtained a phase relationship between the gyrovelocity $\mathbf{v}_\perp$ and the transverse wave field $\delta\mathbf{B}_\perp$ so that energy transfer occurred between the particles and the waves and gyrophase trapping by the wave was possible. Since the field-aligned beam propagate deeply in the foreshock, the local production of gyrating ions through this process should be observed very far from the shock. Meziane et al. (1997) reported the first observations from WIND data of several gyrating ion distributions and their association with low-frequency waves, at distances larger than $20R_E$ from the shock. There was a clear indication of wave–particle interaction. A more detailed study of the three-dimensional ion distributions with a large data set and the highest available time resolution (3 s) has shown that these observational features can be found up to more than $80R_E$ from the shock (Meziane et al., 2001). Investigation of the nonlinear wave trapping mechanism has shown that it can explain the properties of such gyrating ion distributions registered at large distances from the shock (Mazelle et al., 2000). It has been shown that the particle are not only bunched in gyrophase but also trapped in pitch-angle in velocity space around a value which is directly related to the amplitude of the wave self-consistently generated by the original field-aligned ion beam.

In the present paper, we report observations of gyrating ion distribution by Cluster CIS and analyze in great details one particular event. Then we investigate the trapping mechanism to produce such distributions and compare quantitatively the predicted theoretical results with observation. This paper is structured as follows: in the next section, we briefly describe the instrumentation and data analysis; then, we illustrate the observations on particle and low-frequency waves by describing one specific event before analyzing the wave properties; in another section we discuss the interpretation of the observations: first, we discuss the possibility of wave–particle interaction via cyclotron resonance with the local ion distributions; second, we investigate the free energy source for driving an ion/ion instability and solve the linear dispersion relation; third, we discuss a coherent nonlinear wave particle process as a local source mechanism for producing the observed gyrating distribution; the last section is devoted to some conclusions.

2. Instrumentation and data analysis

The particle data used in this study are from Cluster Ion Spectrometer experiment which includes (i) a Hot Ion Analyzer (HIA) which measures particles in the energy range 0.005–26 keV; (ii) a time-of-flight mass spectrometer (CODIF), which combines a top-hat analyzer with a time-of-flight section to measure the major species: H+, He+, He++ and O+. The sensor primarily covers the energy range between 0.02 and 38 keV/q. Both instruments measure full 3D distributions within one satellite spin

period (4 s) with an angular resolution of 22.5° × 22.5°. In normal telemetry mode, one distribution is transmitted every two spins (or three spins depending on the time period), whereas in burst mode the distribution is transmitted every one spin. A detailed description of the Cluster-CIS experiment can be found in the work of Rème et al. (2001). With the above instrumental characteristics both the solar wind plasma as well as the energetic particles are detected. The HIA analyzer operates with high geometry factor (HIA-G) appropriate for upstream ion measurement as well as with low geometry factor (HIA-g) for the solar wind plasma measurements. Our study also uses magnetic field data from the fluxgate magnetometer (FGM) installed on board the Cluster spacecraft (Balogh et al., 2001). We have mainly used low time resolution averaged magnetic field data sufficient to investigate the association of low-frequency waves with the backstreaming ions. Higher resolution magnetic field data (5 vector/s) have also been used for the multi-spacecraft analysis of the low-frequency waves (Eastwood et al., 2002). Finally, we used data registered during polar cusp crossing orbits in spring 2001. For these orbits, the satellites quartet crosses many times the Earth's bow shock and, in the same time, remains relatively close to the shock front. We mainly use data obtained from spacecraft 1. Similar particle dynamics properties are found from observations obtained from spacecraft 3 and 4. During the time of interest all the three spacecrafts were at distances less than 600 km from each other and the spacecraft telemetry mode was a burst mode allowing the highest time resolution for CIS measurements.

We have studied the magnetic fluctuations observed on each of the four spacecraft by using the classical minimum variance analysis (MVA) technique (see e.g., Sonnerup and Scheible, 1998 and references therein). This characterizes the waves, giving the direction of propagation with respect to the background magnetic field $\mathbf{B}_0$, the polarization and the relative wave amplitude $\delta B/B_0$. The usual convention is used to order the eigenvalues of the covariance matrix of the field perturbations $\lambda_1 > \lambda_2 > \lambda_3$ (maximum, intermediate and minimum variances, respectively). The direction of minimum variance gives the direction of propagation with respect to the background magnetic field $\mathbf{B}_0$, computed as the averaged field vector during the time interval analyzed, and provides the angle θ_{kB} between the wave vector $\mathbf{k}$ and $\pm\mathbf{B}_0$. The quality of this determination is measured via the value of the eigenvalue ratio λ_2/λ_3 and then the angular error $\Delta\theta_{kB}$ is usually estimated by assuming that λ_3 represents an isotropic background noise perturbation, which leads to $\Delta\theta_{kB} = \tan^{-1}(\lambda_3/\lambda_2 - \lambda_3)$ (Hoppe et al., 1981). However, Sonnerup and Scheible (1998) do not recommend to use this formula since it does not take into account the number of measured magnetic field vectors used for the analysis. They suggest to instead use for the angular error estimate

$$\Delta\theta_{kB} = \sqrt{\frac{\lambda_3}{(M-1)}\frac{\lambda_2}{(\lambda_2-\lambda_3)^2}},$$

M being the number of vectors. We will use this estimate from MVA for the error on the wave propagation angle. The polarization of the field perturbation can be determined with respect to the ambient field $\mathbf{B}_0$ in the spacecraft frame. Then, the fluctuating levels of the magnetic field and the solar wind proton parameter perturbations have been computed i.e., the magnetic field compression ratio $\delta|\mathbf{B}|/B_0$, the proton density compression ratio $\delta N_p/N_p$ and the $|\delta\mathbf{B}|/B_0$ ratio which characterizes the amplitude of the wave field. Finally, the averaged minimum variance direction deduced from the results of MVA applied on each of the four satellites is compared to the wave vector direction deduced from a multi-spacecraft timing analysis (e.g., Schwartz, 1998). By using the four spacecraft magnetic field data and the averaged solar wind velocity, this analysis provides the wave phase speed in the plasma rest frame as well as the wave number, and thus the wavelength and plasma rest frame angular frequency (Eastwood et al., 2002).

3. Observations

3.1. Overview

Fig. 1 show observations made by Cluster s/c 1 on 07 April 2001 for an interval upstream from the Earth's bow shock which was crossed by s/c 1 at ∼ 21:00 UT and at a radial distance of $13.4R_E$. The two first panels show, respectively, energy-time spectrograms of all ions from CIS/HIA for solar wind sectors (upper panel) and "dusk" solid angle (1π coverage around the—YGSE looking direction—lower panel). The third and fourth panels show interplanetary magnetic field components in GSE coordinates and its magnitude, respectively, from the FGM experiment (4-s averaged data). The three last panels, respectively, display the density and the bulk velocity in GSE coordinates derived by moment calculations from HIA measurements.

Cluster s/c 1 was connected to the bow shock, during a much larger interval. At 2334:30 UT, energetic ions are revealed in the second energy spectrogram corresponding to measurements by the High side of the HIA instrument. The difference with the first panel showing the solar wind population is quite obvious. High fluxes are then continuously observed until 2344 UT, followed by two small patches. These ions are mostly propagating sunward, as revealed from the analysis of their guiding center velocity, i.e., they are backstreaming ions. Before 2334:30 UT, the IMF was nearly quasi-steady. Contrarily, prominent large amplitude low frequency waves are observed after 2335:45 UT. Then the wave amplitude remains very large particularly on the B_y and B_z components (with a peak-to-peak amplitude up to about 15 nT around 2339 UT) until ∼ 2343 UT. The waves are also observed on the solar wind velocity, mainly on the V_z and V_y components (peak-to-peak amplitude up to 100 km/s) as well as on the proton density, which shows their compressive nature.

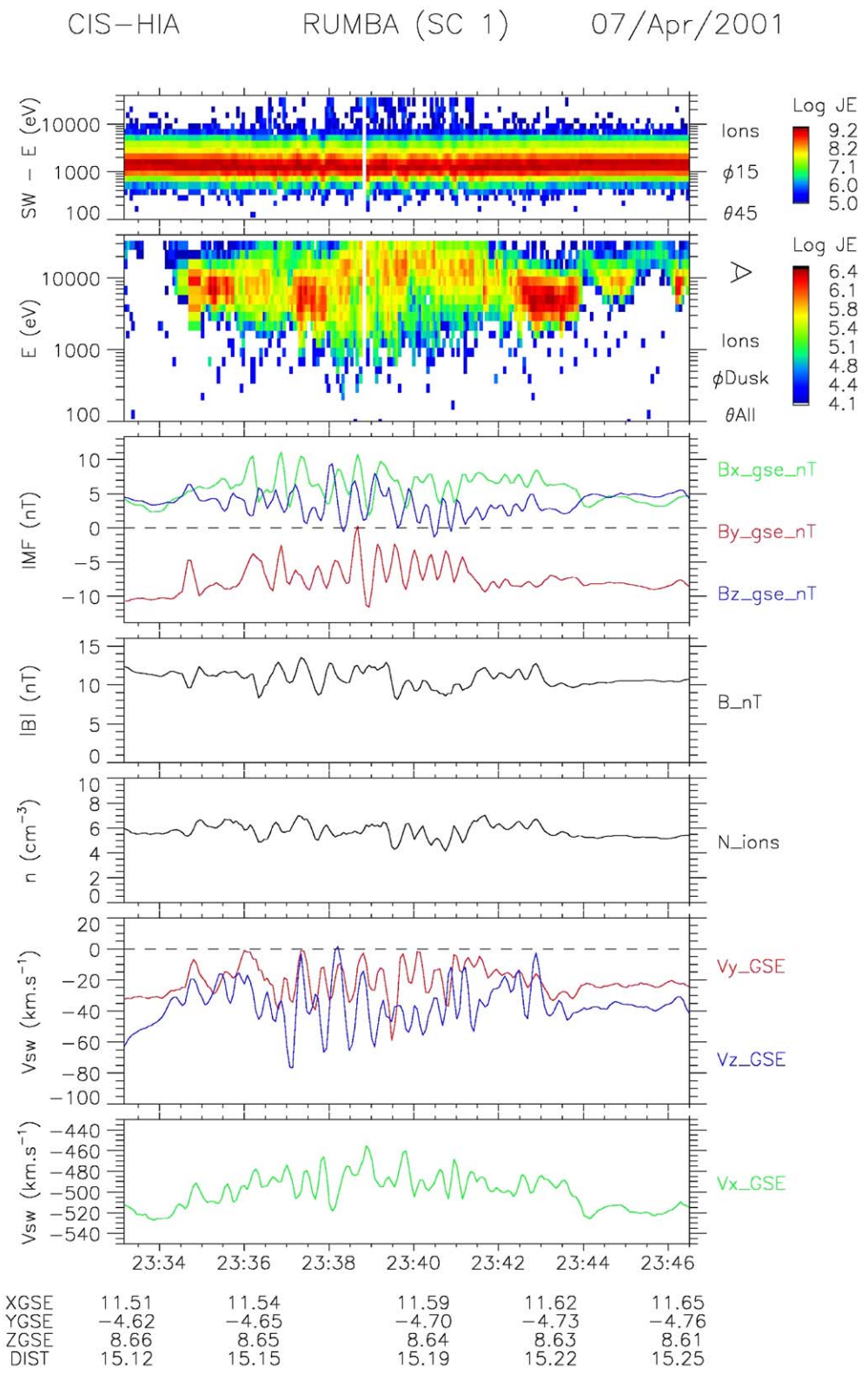

Fig. 1. Observations from CLUSTER CIS and FGM on satellite 1 for an interval upstream from the Earth's bow shock: energy-time spectrograms of all ions from CIS/HIA for "solar wind sectors" (sunward looking direction—upper panel) and "dusk" solid angle (duskward looking direction—second panel), respectively; dc magnetic field components in GSE coordinates and its magnitude; ion density and bulk velocity in GSE coordinates derived from HIA measurements.

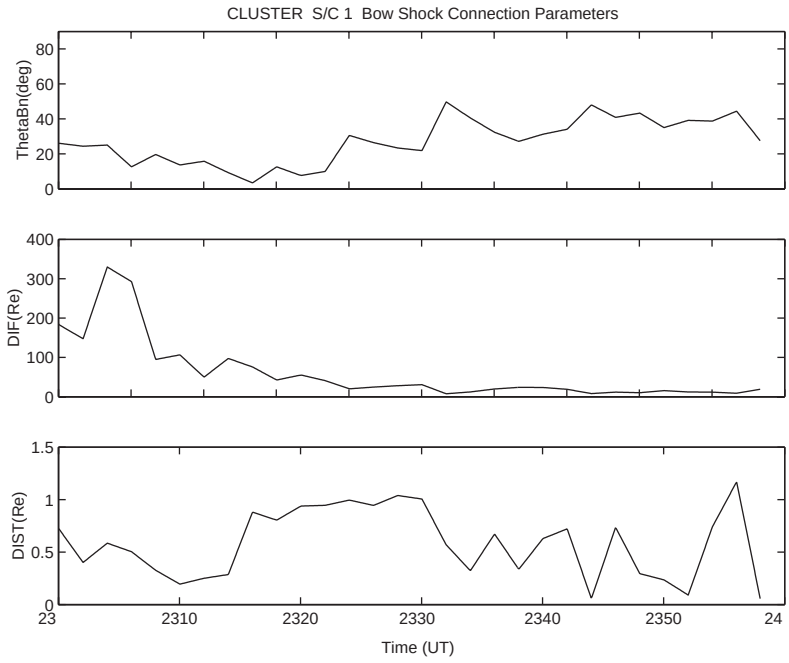

Fig. 2. Bow shock connection parameters computed using CIS and FGM data for satellite 1 using the Cairns et al. (1995) bow shock model (see text). The first panel shows the angle θ_{Bn} between the local normal to the modeled shock surface and the prolonged direction of the IMF at the s/c location, at the intersection point between this direction and the modeled surface (if connection). The second panel shows the distance in Earth radii parallel to the X_{GSE} axis from the s/c to the tangent field line. The third panel shows the distance from the s/c to the intersection point along the IMF direction at the s/c location.

3.2. Shock geometry

Before looking in more details at the particle properties, an estimation of the angle θ_{Bn} as well as the distance from the shock are needed. For this purpose a bow shock model should be adopted. We have used an MHD-based bow shock model reported by Cairns et al. (1995) that namely emphasizes on the MHD effects at low Mach numbers. An average of the magnetic field direction and solar wind density, velocity and ion temperature during the time of interest 2100–2400 UT has been taken for the determination of the bow shock connection parameters. The average Alfvèn speed is $V_A = 92$ km/s. As usual, we have assumed that the averaged magnetic field lines are straight between the spacecraft location and the bow shock. Fig. 2 displays these connection parameters computed using 2-min averaged CIS and FGM data for satellite 1 using the Cairns et al. (1995) bow shock model. The first panel shows the angle θ_{Bn} computed as the angle between the local normal to the modeled shock surface and the prolonged direction of the IMF at the s/c location, at the intersection point between this direction and the modeled surface (if there is connection). The second panel shows the distance parallel to the X_{GSE} axis in Earth radii from the s/c to the tangent field line, giving an idea of the 'depth' inside the foreshock. The third panel shows the distance from the s/c to the intersection point along the IMF direction at the s/c location. This construction of foreshock geometry was pioneered by Greenstadt et al. (1980). These results show that the satellite was mainly connected to the quasi-parallel part of the bow shock, with θ_{Bn} between 20° and 30° for the interval of interest, and was deeply located inside the ion foreshock with a distance from the bow shock much larger than the Larmor radius of protons.

3.3. Ion distributions

Fig. 3 displays three-dimensional 4-s representation of the ion distribution functions registered by CIS-CODIF (burst mode). Nine consecutive distributions are shown for one energy channel ($\sim$ 8 keV) for which the observed backstreaming fluxes are maximum for a time interval inside the event displayed on Fig. 1. For each 4-s interval, a sphere is projected as an elliptic disk to display 4π angular coverage using Hammer–Aitoff projection (Mailing, 1992; Meziane et al., 2001). Each frame represents the normalized phase space density on a surface of constant energy in the solar wind frame of reference. Therefore, each frame in Fig. 3 is a projection in gyrophase and pitch-angle. The **B**-direction is located at the center of each plot and shown by a '+' and pointing outside the page (the anti-field direction is pointed toward the page and indicated by a diamond). The dashed contour plots indicate the projections of the perpendicular mesh of longitude (azimuth) and latitude (polar angle) in the spherical system used; two successive isovalue curves are separated by 45°. The asterisk sign '*' indicates the

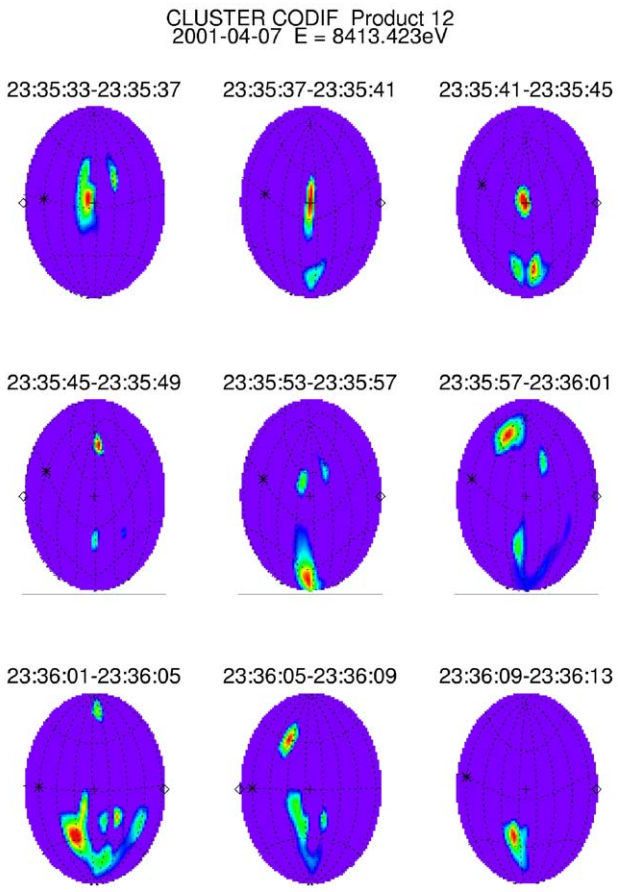

Fig. 3. Sequence of consecutive three-dimensional 4-s display of the proton angular distributions registered by CIS-CODIF (burst mode) for an energy of ~ 8 keV. Each sphere is projected to display 4π-coverage (Hammer–Aitoff projection). The **B** vector is located at the center of each plot (shown by a '+'). The contour plots indicate the pitch-angle isovalues; two successive contours are separated by 45° and the '∗' sign indicates the solar wind direction. Each plot represents the normalized distribution function on a surface of constant energy in the solar wind frame of reference.

solar wind direction corresponding to longitude equal to 180° and latitude equal to zero. For each frame, the maximum value of the normalized phase space density is shown in red.

The first snapshot taken at 2335:33-37 UT indicates an ion beam propagating along the $+\mathbf{B}$ direction with a parallel velocity of 1100 km/s. The two following snapshots also reveal field-aligned ion beams but the third one also shows a second peak for a large pitch-angle of about 60°. Then after 2335:45, the spacecraft has entered a gyrating ion region. Gyrating ions are identified by their gyrophase-restricted distribution peaked off the magnetic field direction. We mention that the interplanetary magnetic field used to plot the distributions is averaged over the spin interval (4 s) while the local proton cyclotron period is 7 s (i.e., about two ion sampling intervals). The gyrating distributions show a clear rotation of their maximum phase density in the left-handed sense around the magnetic field with alternating values separated by about 180°. Such gyrating ion distributions are observed up to ~2344 UT.

3.4. Low-frequency wave properties

The prominent large amplitude low-frequency waves displayed in the third panel of Fig. 1 on the dc magnetic field components appear after 2335:45 UT, the very time when the energetic backstreaming ion distributions on Fig. 3 change from field aligned beam-like to (gyrophase bunched) ring-like shape. The observed period in the spacecraft frame, computed from the mean interval between magnetic field wave crests for all components, is 25 ± 2 s while the local proton gyroperiod is about 7 s.

We have first studied the magnetic fluctuations observed on each of the four spacecraft by using the MVA technique. Fig. 4 illustrates the results obtained for satellite 1, for the time interval 2337:51–2339:51 UT. The upper left panel shows the time sequences of the magnetic field components in the principal axes coordinate system and the other panels the corresponding hodograms. Despite the large amplitude of the waves, the waveform is regular and quasi-monochromatic and the hodograms reveal that the wave field vector remains in a well-defined plane with a very accurate determination of its normal vector ($\lambda_2/\lambda_3 = 49.5$), which leads to $\Delta\theta_{kB} \cong 1°$. The minimum variance direction is $\mathbf{e}_{\min} = [0.700; -0.605; 0.380]$ in GSE coordinates. This provides a direction of propagation nearly parallel to the ambient magnetic field $\mathbf{B}_0$, computed as the averaged field for the time interval studied ($\theta_{kB} = 7 \pm 1°$). The waves are nearly circularly ($\lambda_1/\lambda_2 \approx 1.7$) and left-hand polarized with respect to $\mathbf{B}_0$ in the spacecraft frame, as shown on the hodogram in the principal variance plane, with an observed period (Doppler-shifted) much larger than the local proton gyroperiod. As expected, the computed total wave amplitude is very large ($|\delta\mathbf{B}|/B_0 \approx 1$). The wave is mainly transverse ($|\delta\mathbf{B}_\perp|/B_0 = 0.85$) but the compressive component is not negligible with $\delta|\mathbf{B}_\parallel|/B_0 \approx \delta|\mathbf{B}|/B_0 = 0.45$ comparable with the relative proton density variation $\delta N_p/N_P \sim 0.32$. The low-frequency waves observed on the interplanetary magnetic field on the three other satellites are very similar and consequently the results obtained by the MVA technique are very similar. The angle between the four spacecraft averaged magnetic field and the averaged MVA direction ($\mathbf{e}_{\mathrm{mva}} = (0.734; -0.590; 0.334)$) is 5.1°. The multi-spacecraft timing analysis techniques (Eastwood et al., 2002; Eastwood et al., 2003) provide a very similar wave vector direction $\mathbf{e}_k = \mathbf{k}/|\mathbf{k}| = [0.696; 0.542; 0.472]$, which gives a value of $\theta_{kB} = 5.3°$ with the four spacecraft averaged magnetic field direction. The phase speed in the solar wind frame is $V_\phi = 100 \pm 10$ km/s very close to the local value of the Alfvèn speed $V_A = 98$ km/s, which leads to a wave frequency $\omega/2\pi = 0.014$ Hz while the cyclotron frequency is $\Omega_p/2\pi = 0.143$ Hz, and the associated parallel

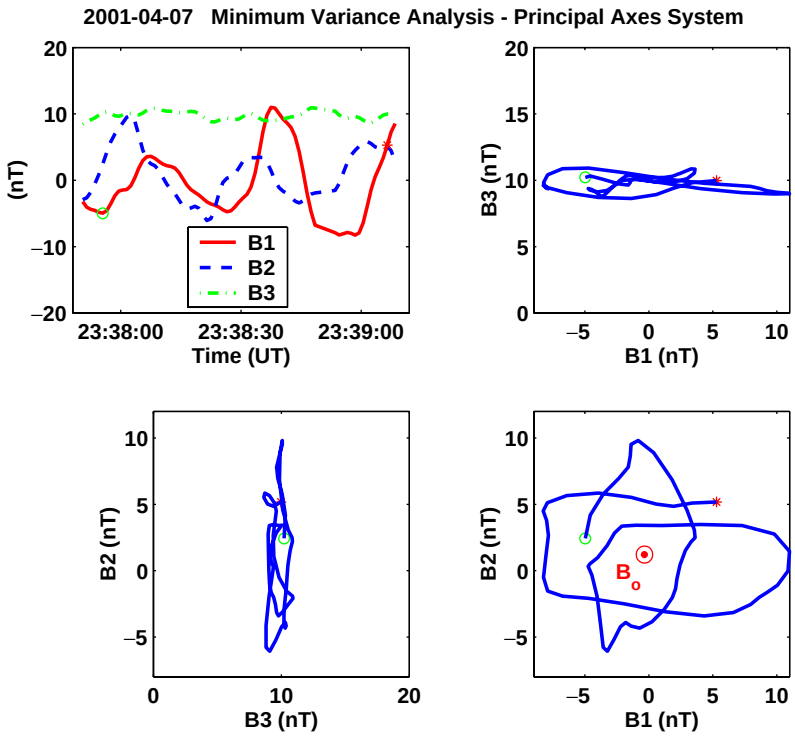

Fig. 4. Components (upper left) and corresponding hodograms of the low-frequency wave magnetic field in the principal axes coordinates derived from a minimum variance analysis for the event shown on Fig. 1 for satellite 1. The open circle (asterisk), respectively, indicate the beginning (end) of each hodogram.

wavelength is $\lambda_{exp} = 7000 \pm 300$ km $\sim 1.05 R_E$. The very similar wave pattern between the different spacecraft of the Cluster tetrahedron is thus not surprising taking into account the large wavelength compared to the spacecraft separation at the time of the observations. Note also that these foreshock LF waves have very common properties compared to previous observations (e.g., Fuselier et al., 1986c): they are mainly transverse, propagating close to the background field with a phase velocity close to the Alfvèn speed and co-streaming with the foreshock backstreaming particles, i.e., mainly against the solar wind flow (so that there are subject to anomalous Doppler shift and polarization reversal from the plasma frame to the s/c frame, as detailed later, implying that they are right-hand mode waves) with a frequency in the plasma frame that is typically $\Omega_p/10$, and a wavelength of the order of one Earth's radius.

3.5. Interpretation

3.5.1. Possibility of cyclotron resonance

In agreement with earlier investigations (Thomsen et al., 1985; Fuselier, 1994; Mazelle et al., 2000; Meziane et al., 2001), the gyrating ion distributions discussed here are always associated with such highly transverse weakly compressive low-frequency waves propagating at small angles relative to the IMF. The angle θ_{kV} between the wave vector and the solar wind velocity has been computed by using the proton velocity averaged over the time interval studied. It can be noted that this angle is 135°, which implies a propagation upstream in the solar wind frame. To investigate as quantitatively as possible the possibility of local resonance between the observed waves and gyrating ion populations, we compare the observed wave periods T_{obs} with the periods T_{pred} one would predict in the spacecraft frame for waves in cyclotron resonance with the locally observed distributions.

Consideration on the branches of the dispersion relation in the Brillouin plane helps to determine what kind of wave mode is a good candidate for cyclotron resonance (e.g., Brinca, 1991). The waves are quasi-monochromatic with large amplitudes and mainly transverse which is consistent with earlier statistical studies (Fuselier et al., 1986c). The variations of the ion density appear correlated with the magnetic field magnitude for all the interval shown in Fig. 1, which is a property of the fast magnetosonic mode in the MHD limit. The properties of the associated waves could first lead to search for wave excitation by an initial gyrophase-bunched ion (i.e., a highly nongyrotropic). For a wide range of values for the mean pitch angle of the gyrating ions, the instability which gives rise to the largest growth rate is the ion/ion right-hand helical beam instability (e.g., Gary, 1991, and references therein). This type of instability has also largely been reported around comets, generated from the newborn ions at the heavy ion gyrofrequency (e.g., Brinca, 1991; Tsurutani, 1991, and references therein; Cao

et al., 1995, 1998) as well as at the proton gyrofrequency (Mazelle and Neubauer, 1993). The wave mode is necessarily a right-hand mode co-streaming with the ions along the ambient magnetic field, i.e., towards the sun, so that it can resonate with a backstreaming ion population ($\mathbf{k}\cdot\mathbf{V}_{\|}$ must be positive). In the MHD limit, this mode is the magnetosonic mode, and its phase velocity is of the order of the local Alfvèn speed, i.e., much smaller than the parallel ion speed $V_{\|}$ which is always larger than V_{sw}. Therefore, the ion beam overtakes the waves so that there is an anomalous Doppler shift in their reference frame: the ions sense left-handed waves. Considering the small spacecraft velocity relative to the Earth, the proton right-hand mode waves are also observed in the spacecraft frame as left-handed waves (Hoppe and Russell, 1983). Moreover, for the MHD limit of this type of low-frequency (magnetosonic) waves, the group velocity is parallel to the magnetic field with the same sense as $\mathbf{k}_{\|}$; therefore the wave energy (the Poynting flux) is driven away from the Earth environment in the solar wind frame toward the sun, contrarily to solar wind originated waves. This is fully consistent with the observed value of θ_{kV}.

The cyclotron resonance condition with the right-hand mode writes

$$\omega - k_{\|}V_{\|} + \Omega_{\mathrm{p}} = 0, \tag{1}$$

where ω is the wave frequency in the solar wind rest frame, Ω_{p} is the proton gyrofrequency, $k_{\|}$ is the component of the wave vector parallel to the background magnetic field, and $V_{\|}$ is the parallel component of the resonant ion velocity (solar wind frame). By first assuming $\omega \ll \Omega_{\mathrm{p}}$, we can make the approximation

$$k_{\|} \approx \frac{\Omega_{\mathrm{p}}}{V_{\|}}. \tag{2}$$

In the spacecraft frame, these waves would have a Doppler-shifted frequency of

$$\omega' = \omega + \mathbf{k}\cdot\mathbf{V}_{sw} \approx k_{\|}V_{sw}\frac{\cos\theta_{kV}}{\cos\theta_{kB}}. \tag{3}$$

Then using the experimental values, we have computed the predicted wave periods $T_{\mathrm{pred}} \equiv 2\pi/\omega'$ according to (2) and (3) and compared it with the observed period T_{obs}. For instance, for 2337:01 UT, the gyrating proton distribution has a parallel velocity $V_{\|} = 900 \pm 100$ km/s, which gives $T_{\mathrm{pred}} = 20 \pm 2$ s while $T_{\mathrm{obs}} = 25 \pm 2$ s. For all the ion distributions in this interval the associated predicted periods are systematically smaller but close to the observed value, taking into account the experimental uncertainties. The deduced parallel wavelengths $\lambda_{\|}$ of these predicted resonant waves all are of the order of $1R_{\mathrm{E}}$, which is consistent with the above results. Moreover, if one assumes exact local cyclotron resonance with the local waves solving the linear system made by (1) and (3) without any approximation, this leads for the above example to a wave frequency in the plasma frame $\omega/\Omega_{\mathrm{p}} = 0.124$, a phase velocity $V_{\phi} = 110$ km/s $\sim V_{\mathrm{A}}$ and a parallel wavelength $\lambda_{\|} = 6000$ km, i.e., wave properties different but close to those observed, $\omega_{\mathrm{exp}}/\Omega_{\mathrm{p}} = 0.1$, $V_{\phi\,\mathrm{exp}} = 100 \pm 10$ km/s and $\lambda_{\mathrm{exp}} = 7000 \pm 300$ km, respectively. This strongly supports the possibility that local cyclotron resonant interaction with the waves occurs for these distributions. These waves propagating upstream in the solar wind frame at a phase speed much smaller than V_{sw} are simply blown back by the solar wind and interact with the local backstreaming distributions leaking upstream with a much larger parallel velocity ($V_{\|} \sim 10V_{\mathrm{A}}$, typically). Although the ring-beam distributions still contains a large amount of free energy to generate this kind of wave (e.g., Killen et al., 1995), this does not necessarily imply, however, that the waves are locally produced by the observed distributions.

Moreover, a more careful analysis reveals that the observed parallel velocities of the local gyrating distributions generally appear a little bit too small for T_{pred} to match T_{obs}. As revealed in Fig. 3, field-aligned beams are clearly observed just before the ring-like distributions and their characteristics can be derived. We then make the same test of period matching for the field-aligned beams. To illustrate that, for the distribution dated from 2335:37 UT in Fig. 3, $V_{\|} = 1060 \pm 50$ km/s which gives $T_{\mathrm{pred}} = 25.4$ s while $T_{\mathrm{obs}} = 25 \pm 2$ s . Moreover, if one solves the linear system made by (1) and (3) without any approximation, assuming exact local cyclotron resonance, this leads for the above example to a wave frequency $\omega/\Omega_{\mathrm{p}} = 0.103$, a phase velocity $V_{\phi} = 99$ km/s $\approx V_{\mathrm{A}}$ and a parallel wavelength $\lambda_{\|} = 7000$ km, i.e., wave properties which are a much better match to those observed. Thus, such a beam distribution could have generated the observed wave from the resonant right-hand ion/ion beam instability (e.g., Gary, 1991; Fuselier et al., 1986b).

3.5.2. Linear theory

To test this hypothesis, we solve the linear Maxwell–Vlasov dispersion relation for parallel electromagnetic modes by using the WHAMP program (Rönmark, 1982). We use a plasma model with parameters using the CLUSTER observations: $N_{\mathrm{p}} = 6$ cm^{-3}, $N_{\mathrm{beam}} = 7.10^{-3}$ cm^{-3}, $T_{\mathrm{e}} = 7$ eV, $T_{\mathrm{p}} = 8$ eV, $V_{\|\mathrm{beam}} = 1060$ km/s, $T_{\mathrm{beam}} = 130$ eV, $V_{\mathrm{ALFVÈN}} = 98$ km/s. As expected only the ion/ion right-hand mode is found to be unstable for the local plasma parameters. The results are shown in Fig. 5. The real frequency at the growth rate maximum is $\omega_{\mathrm{max}}/\Omega_{\mathrm{p}} = 0.097$ and $\gamma_{\mathrm{max}}/\Omega_{\mathrm{p}} = 0.052$. This value could be compared with the analytical approximation of this linear growth rate given by Gary (1981), $\gamma_{\mathrm{max}}/\Omega_{\mathrm{p}} = (n_{\mathrm{beam}}/2n_{\mathrm{e}})^{1/3} = 0.084$, but this approximation holds only for $0.01 \leqslant n_{\mathrm{beam}}/n_{\mathrm{e}} \leqslant 0.1$ while here $n_{\mathrm{beam}}/n_{\mathrm{e}} = 1.2 \times 10^{-3}$. The phase velocity is $V_{\phi} = 1.097V_{\mathrm{A}}$ (107 km/s), in very good agreement with the value in the plasma frame computed from the observations (100 km/s). The associated parallel wavelength is $\lambda_{\mathrm{max}} = 6670$ km, in very good agreement with the experimental value $\lambda_{\mathrm{exp}} = 7000 \pm 300$ km $\sim 1.05R_{\mathrm{E}}$. This helps to conclude that the observed field-aligned beam or at least a beam with similar properties (density, drift velocity and

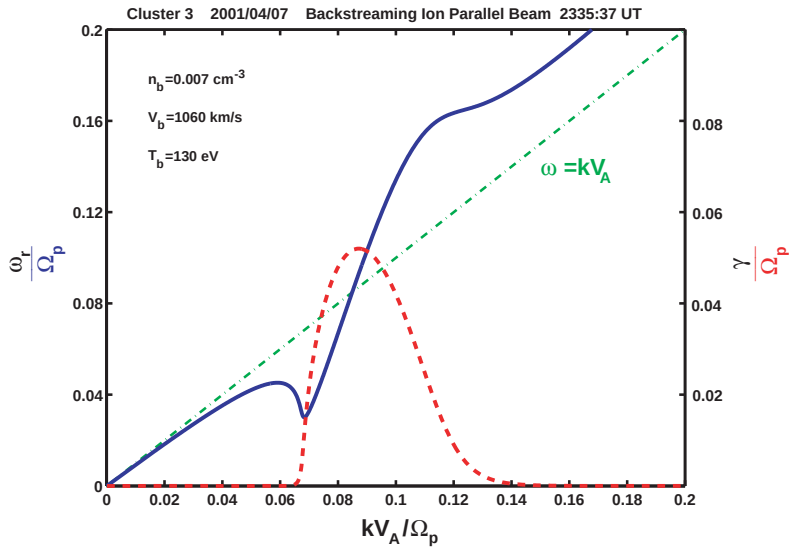

Fig. 5. Real frequency (solid line) and growth rate (dashed line) of the ion/ion right-hand resonant instability as functions of the normalized wave number at propagation parallel to $\mathbf{B}_0$ for experimental parameters suitable for the field-aligned beam distribution shown on the second display of Fig. 3.

temperature) is a very good candidate to be the source of the waves observed with the gyrating ion distributions.

3.5.3. Nonlinear wave–particle trapping

Among the gyrating ion distributions reported, no event is consistent with a specular reflection at the Earth's bow shock since their observed pitch-angles are much too large (it should be nearly θ_{Bn} (e.g., Schwartz et al., 1983)). It is thus necessary to invoke a local production mechanism for these upstream distributions. The predicted wave periods in the s/c frame for cyclotron resonance with right-hand mode waves are close to the observed periods. This is a clear indication of wave–particle interaction. Field-aligned beams observed in the region just adjacent to region of gyrating distributions (see Fig. 3) appear even in closer cyclotron resonance with the ULF waves observed later simultaneously with the gyrating ions. Results of the linear theory show that the field-aligned beams are very good candidates to generate the waves. Thus, it is quite natural to check the validity of a possible scenario implying wave generation from the ion beam instability and nonlinear beam disruption by the excited wave to produce the observed gyrophase-bunched distributions.

For this, we make some theoretical considerations about the nonlinear trapping of ions by an electromagnetic monochromatic wave. From the equation of motion of a particle of velocity $\mathbf{v}$ in the frame moving along the dc magnetic field $\mathbf{B}_0(\|z)$ at the phase velocity $V_\phi\,(\ll c)$ a monochromatic wave, propagating along $\mathbf{B}_0$ with a constant amplitude B_1, it is easy to deduce two constants of the motion (e.g., Roux and Solomon, 1970; Gendrin 1974; Matsumoto, 1985; Le Quéau and Roux, 1987):

$$T = w_\parallel^2 + w_\perp^2 = C_1 \tag{4}$$

and

$$S = (w_\parallel - 1)^2 - 2\frac{\Omega_1}{\Omega_0} w_\perp \sin\psi = C_2, \tag{5}$$

where $\mathbf{w} = k_\parallel/\Omega_0\mathbf{v}$, $\Omega_{0,1} = qB_{0,1}/m$, $\psi = \varphi + k_\parallel z$ and φ is the gyrophase angle. The invariance of T is simply the conservation of total particle energy in the wave frame (no electric field in this frame). The invariant S relates the parallel and perpendicular motion of the particles. Using the particle equations of motion with (4) and (5), it is possible to show that S can be used as a Hamiltonian of the particle motion and that the system is solvable by a quadrature

$$\frac{\mathrm{d}w_\parallel}{\mathrm{d}t} = \pm\frac{\Omega_0}{2} \times\sqrt{4\left(\frac{\Omega_1}{\Omega_0}\right)^2 \sin^2\psi(C_1 - w_{||}^2) - [(w_{||}-1)^2 - C_2]^2},$$

which can be solved in terms of elliptic integrals as for a pendulum equation. The particle is thus trapped in a potential well.

Using the pitch-angle α such as $\tan\alpha = w_\perp/w_\parallel$, the equations of motions

$$\mathrm{d}\alpha/\mathrm{d}t = -\delta\cos\psi \tag{6}$$

and

$$\frac{\mathrm{d}\psi}{\mathrm{d}t} = \delta\cot\alpha\sin\psi + \sqrt{T}\cos\alpha - 1, \tag{7}$$

where

$$\delta = \frac{\Omega_1}{\Omega_0} = \frac{\delta B_\perp}{B_0} \tag{8}$$

can be derived from the Hamiltonian $S(\alpha,\psi)$.

Table 1
Experimental parallel and perpendicular velocity and associated pitch-angles in the wave frame (using the experimental wave phase speed of 100 km/s) for some observed gyrating ion distributions ($\alpha_{0\,\mathrm{theory}} = 59.8°$)

Time (UT)	$V_{\parallel}$ (km/s)	$V_{\perp}$ (km/s)	α_{exp} (deg)
23:38:09	500	910	66
23:38:13	600	855	60
23:38:25	650	815	56
23:38:29	700	1060	60
23:38:45	600	845	59

This Hamiltonian has a singularity for $\psi_0 = \pi/2$ which is the only to be considered since the pitch angle α is defined in the interval $[0, \pi]$. As a first step, we consider a mono energetic parallel ion beam, i.e., this means from Eqs. (2), (4) and (6) that we have $T = 1$. Then, by linearizing the trapping potential, around $\psi_0 = \pi/2$, it is straightforward to show that this singularity corresponds to a value α_0, defining the center of the trapping cells. For small values of α_0, it is possible to use the approximation $\alpha_0 \approx (2\delta)^{1/3}$. If $V_{\parallel 0}$ is the initial velocity of the cyclotron resonant beam (i.e., $T = 1$), the nonlinear interaction will tend to create a peak in the distribution around the center of the trapping cell in phase space associated with the pitch angle α_0.

To illustrate this, we use the experimental results described above. We use the experimental parallel and perpendicular velocities for some observed gyrating ion distributions corresponding to the time interval where we have analyzed the low-frequency waves to compute the associated pitch-angles in the wave frame (using the experimental wave phase speed of 100 km/s). Table 1 helps to compare these values with the theoretical value which is $\alpha_{0\,\mathrm{theory}} = 59.8°$ using the mean value $\delta = 0.85$ from the observations.

The very good agreement obtained strongly suggests the possible scenario that the quasi-monochromatic wave generated from the ion/ion beam instability could then have nonlinearly trapped the ions to produce the resulting gyrating distributions.

4. Conclusion

We have investigated a local production mechanism to explain the existence of the well-defined gyrating ion distributions reported from the Cluster CIS measurements in the Earth's foreshock. We have analyzed the associated large amplitude low frequency waves using multi-spacecraft analysis techniques and show that they are consistent with right-hand mode waves in the plasma frame (anomalous Doppler shift) that can be in interaction with the ions through cyclotron resonance. We have studied the possibility of resonantly driving these waves unstable from the electromagnetic ion/ion beam instability by field-aligned beam ions also observed in the same region. The results from the linear theory lead to a very good agreement with the observed wave mode. Then the possibility of producing the observed gyrophase-bunched ion distributions from the disruption of the beam by the excited wave has led to a good quantitative agreement from nonlinear trapping theory. This result is very similar to those obtained from previous studies in the distant foreshock (up to $80R_E$ from Wind data with lower backstreaming ion densities and wave amplitude (Meziane et al., 1997, 2001; Mazelle et al., 2000), which could mean that the present case study corresponds to the same mechanism observed by Cluster closer to the bow shock. Other events consistent with this trapping mechanism have also been identified but it must be mentioned that all the gyrating events already registered by CIS cannot be explained by this mechanism. Gyrophase-bunched ions produced by specular reflection have also been identified (Mazelle et al., 2002; Meziane et al., 2003, manuscript in preparation). But a better statistics is necessary to determine the percentage of gyrating events corresponding to either mechanism. It will be also interesting then to examine the location of such events and compare them with the forward boundary of the foreshock ULF waves studied by Le and Russell (1992).

Acknowledgements

C.M. and K.M. thanks I.H. Cairns for providing the code for the bow shock model and E. Penou for his assistance. C.M. also thanks G. Belmont and L. Rézeau for providing an elaborated version of the WHAMP program.

References

Balogh, A., Carr, C.M., Acuña, M.H., Dunlop, M.W., Beek, T.J., Brown, P., Fornacon, K.-H., Georgescu, E., Glassmeier, K.-H., Harris, J., Musmann, G., Oddy, T., Schwingenschuh, K., 2001. The cluster magnetic field investigation: overview of in-flight performance and initial results. Ann. Geophysicae 19, 1207–1217.

Bonifazi, C., Moreno, G., 1981a. Reflected and diffuse ions backstreaming from the Earth's bow shock 1, basic properties. J. Geophys. Res. 86, 4381–4396.

Bonifazi, C., Moreno, G., 1981b. Reflected and diffuse ions backstreaming from the Earth's bow shock 2, origin. J. Geophys. Res. 86, 4397–4404.

Brinca, A.L., 1991. In: Johnstone, A.D. (Ed.), Cometary Linear Instabilities: From Profusion to Prospective, Geophysical Monograph Series, Vol. 61. AGU, Washington, DC, pp. 211–221.

Cairns, I.H., Fairfield, D.H., Anderson, R.R., Carlton, V.E.H., Paularena, K.I., Lazarus, A.J., 1995. Unusual locations of earth's bow shock on September 24–25, 1987: Mach number effects. J. Geophys. Res. 100, 47–62.

Cao, J.B., Mazelle, C., Belmont, G., Rème, H., 1995. The nongyrotropy of heavy newborn ions at comet Grigg–Skjellerup and corresponding instability. J. Geophys. Res. 100, 23,379–23,388.

Cao, J.B., Mazelle, C., Belmont, G., Rème, H., 1998. Oblique ring instability driven by nongyrotropic ions: application to observations at comet Grigg–Skjellerup. J. Geophys. Res. 103, 2055–2067.

Eastwood, J.P., Balogh, A., Dunlop, M.W., Horbury, T.S., Dandouras, I., 2002. Cluster observations of fast magnetosonic waves in the terrestrial foreshock. Geophys. Res. Lett. 29 (22), 2046.

Eastwood, J.P., Balogh, A., Lucek, E., Mazelle, C., Dandouras, I., 2003. On the existence of Alfvèn waves in the terrestrial foreshock. Annales Geophys. 21, 1457–1465.

Fazakerley, A.N., Coates, A.J., Dunlop, M.W., 1995. Observations of upstream ions, solar wind ions and electromagnetic waves in the Earth's foreshock. Adv. Space Res. 15 (8/9), 103–106.

Fuselier, S.A., 1994. Suprathermal Ion Upstream and Downstream From the Earth's Bow Shock, Geophysical Monograph, Vol. 81. pp. 107–119.

Fuselier, S.A., Gosling, J.T., Thomsen, M.F., 1986a. The motion of ions specularly reflected off a quasi-parallel shock in the presence of large-amplitude, monochromatic MHD waves. J. Geophys. Res. 91, 4163–4170.

Fuselier, S.A., Thomsen, M.F., Gary, S.P., Bame, S.J., Russell, C.T., Parks, G.K., 1986b. The phase relationship between gyrophase-bunched ions and MHD-like waves. Geophys. Res. Lett. 13, 60–63.

Fuselier, S.A., Thomsen, M.F., Gosling, J.T., Bame, S.J., Russell, C.T., 1986c. Gyrating and intermediate ion distributions upstream from the earth's bow shock. J. Geophys. Res. 91, 99.

Gary, S.P., 1991. Electromagnetic ion/ion instabilities and their consequences in space plasmas: a review. Space Science Reviews 56, 373–415.

Gary, S.P., Gosling, J.T., Forslund, D.W., 1981. The electromagnetic ion beam instability upstream of the Earth's bow shock. J. Geophys. Res. 86, 6691–6696.

Gendrin, R., 1974. Phase-bunching and other non-linear processes occurring in gyroresonant wave-particle interactions. Astrophysics and Space Science 28, 245–266.

Gosling, J.T., Asbridge, J.R., Bame, S.J., Paschmann, G., Sckopke, N., 1978. Observations of two distinct population of bow shock ions in the upstream solar wind. Geophys. Res. Lett. 5, 957–960.

Gosling, J.T., Thomsen, M.F., Bame, S.J., Feldman, W.C., Paschmann, G., Sckopke, N., 1982. Evidence for speculary reflected ions upstream from the quasi-parallel bow shock. Geophys. Res. Lett. 87, 1333–1336.

Greenstadt, E.W., Mellott, M.M., 1985. Variable field-to-normal shock-foreshock boundary observed by isee-1 and -2. Geophys. Res. Lett. 12, 129–132.

Greenstadt, E.W., Russell, C.T., Hoppe, M., 1980. Magnetic field orientation and suprathermal ions streams in the earth's foreshock. J. Geophys. Res. 85, 3473.

Gurgiolo, C., Parks, G.K., Mauk, B.H., Lin, C.S., Anderson, K.A., Lin, R.P., Rème, H., 1981. Non-E_B ordered ion beams upstream of the Earth's bow shock. J. Geophys. Res. 86, 4415.

Gurgiolo, C., Parks, G.K., Mauk, B.H., 1983. Upstream gyrophase bunched ions: a mechanism for creation at bow shock and the growth of velocity space structure through gyrophase mixing. J. Geophys. Res. 88, 9093–9100.

Hoppe, M.M., Russell, C.T., Frank, L.A., Eastman, T.E., Greenstadt, E.W., 1981. Upstream hydromagnetic waves and their association with backstreaming ion populations: isee-1 and -2 observations. J. Geophys. Res. 86, 4471–4492.

Hoppe, M.M., Russell, C.T., 1983. Plasma rest frame frequencies and polarizations of the low-frequency upstream waves – isee-1 and -2 observations. J. Geophys. Res. 88, 2021–2027.

Hoshino, M., Terasawa, T., 1985. Numerical study of the upstream waves excitation mechanism, 1, nonlinear phase bunching of beam ions. J. Geophys. Res. 90, 564–573.

Killen, K., Omidi, N., Krauss-Varban, D., Karimabadi, H., 1995. Linear and nonlinear properties of ULF waves driven by ring beam distribution functions. J. Geophys. Res. 100, 4342–5835.

Le, G., Russell, C.T., 1992. A study of ULF wave foreshock morphology-I: ULF foreshock boundary. Planet. Space Sci. 40, 1203–1213.

Lee, M.A., 1982. Coupled hydromagnetic wave excitation and ion acceleration upstream of the Earth's bow shock. J. Geophys. Res. 87, 5063–5080.

Le Quéau, D., Roux, A., 1987. Quasi-monochromatic wave-particle interactions in magnetospheric plasmas. Solar Phys. 111, 59–80.

Mailing, D.H., 1992. Coordinate Systems and Map Projections, 2nd Edition. Pergamon, Tarrytown, NY.

Matsumoto, H., 1985. Coherent nonlinear effects on electromagnetic wave–particle interactions. Space Sci. Rev. 42, 429–448.

Mazelle, C., Neubauer, F.M., 1993. Discrete wave packets at the proton cyclotron frequency at comet P/Halley. Geophys. Res. Lett. 20, 153–156.

Mazelle, C., Le Quéau, D., Meziane, K., 2000. Nonlinear wave particle interactions due to quasi-monochromatic ULF waves in the Earth foreshock. Nonlinear Proces. Geophys. 7, 185–190.

Mazelle, C., et al., 2002. Bow shock specular reflected ions in the presence of low frequency electromagnetic waves: a case study. Eos Trans. AGU 83(47) (Fall Meet. Suppl.) Abstract SH72A-0550.

Meziane, K., et al., 1997. Wind observations of gyrating ion distributions and low frequency waves upstream from the Earth's Bow Shock. Adv. Space Res. 20 (4), 703–706.

Meziane, K., Mazelle, C., Lin, R.P., LeQuéau, D., Larson, D.E., Parks, G.K., Lepping, R.P., 2001. Three-dimensional observations of gyrating ion distributions far upstream from the earth's bow shock and their associated with low-frequency waves. J. Geophys. Res. 106, 5731–5742.

Paschmann, G., Sckopke, N., Asbridge, J.R., Bame, S.J., Gosling, J.T., 1980. Energization of solar wind ions by reflection from the Earth's bow shock. J. Geophys. Res. 85, 4689–4693.

Paschmann, G., Sckopke, N., Papamastorakis, I., Asbridge, J.R., Bame, S.J., Gosling, J.T., 1981. Characteristics of reflected and diffuse ions upstream from the Earth's bow shock. J. Geophys. Res. 86, 4355–4364.

Rème, H., Aoustin, C., Bosqued, J.M., Dandouras, I., Lavraud, B., Sauvaud, J.A., Barthe, A., Bouyssou, J., Camus, T., Coeur-Joly, O., Cros, A., Cuvilo, J., Ducay, F., Garbarowitz, Y., Medale, J.L., Penou, E., Perrier, H., Romefort, D., Rouzaud, J., Vallat, C., Alcayde, D., Jacquey, C., Mazelle, C., d'Uston, C., Möbius, E., Kistler, L.M., Crocker, K., Granoff, M., Mouikis, C., Popecki, M., Vosbury, M., Klecker, B., Hovestadt, D., Kucharek, H., Kuenneth, E., Paschmann, G., Scholer, M., Sckopke, N., Seidenschwang, E., Carlson, C.W., Curtis, D.W., Ingraham, C., Lin, R.P., McFadden, J.P., Parks, G.K., Phan, T., Formisano, V., Amata, E., Bavassano-Cattaneo, P., Baldetti, M.B., Bruno, R., Chionchio, G., Di Lellis, A., Marcucci, M.F., Pallocchia, G., Korth, A., Daly, P.W., Graeve, B., Rosenbauer, H., Vasyliunas, V., McCarthy, M., Wilber, M., Eliasson, L., Lundin, R., Olsen, S., Shelley, E.G., Fuselier, S., Ghielmetti, A.G., Lennartsson, W., Escoubet, C.P., Balsiger, H., Friedel, R., Cao, J.-B., Kovrazhkin, R.A., Papamastorakis, I., Pellat, R., Scudder, J., Sonnerup, B.U.O., 2001. First multispacecraft ion measurements in and near the Earth's magnetosphere with identical cluster ion spectrometry (cis) experiment. Ann. Geophys. 19, 1303–1354.

Rönmark, K., 1982. WHAMP-waves in homogeneous, anisotropic multicomponent plasmas. Report No. 179, Kiruna Geophysics Institute, Kiruna, Sweden.

Roux, A., Solomon, J., 1970. Mécanismes non linéaires associés aux interactions ondes-particules dans la magnétosphère. Ann. Geophys. 2, 279–297.

Schwartz, S.J., Thomsen, M.F., Gosling, J.T., 1983. Ions upstream of the Earth's bow shock: a theoretical comparison of alternative source populations. J. Geophys. Res. 88, 2039–2047.

Schwartz, S.J., 1998. Shock and discontinuity normals. Mach numbers and related parameters. In: Paschmann, G., Daly, W., (Eds.), Analysis Methods for Multi-spacecraft Data. ISSI Scientific Report.

Sonnerup, U.Ö., Scheible, M., 1998. Minimum and maximum variance analysis. In: Paschmann, G., Daly, W., (Eds.), Analysis Methods for Multi-spacecraft Data. ISSI Scientific Report.

Thomsen, M.F., Gosling, J.T., Bame, S.J., Russell, C.T., 1985. Gyrating ions and large-amplitude monochromatic MHD waves upstream of the Earth's bow shock. J. Geophys. Res. 90, 267–273.

Tsurutani, B.T., 1991. Comets: a laboratory for plasma waves and instabilities, cometary plasma processes. In: Johnstone, A.D., (Eds.), The American Geophys. University press, Washington, DC.